Ocean control on sea ice in the Nordic Seas

Wanyee Wong[1], Bjørg Risebrobakken[1], Malin Ödalen[1], Amandine Aline Tisserand[1], Kirsten Fahl[3], Ruediger Stein[3,4,5], Eystein Jansen[1,2]

[1]NORCE Norwegian Research Centre, Bjerknes Centre for Climate Research, 5007 Bergen, Norway
5   [2]Department of Earth Science, University of Bergen, Bjerknes Centre for Climate Research, 5007 Bergen, Norway
[3]Alfred Wegener Institute, Helmholtz Centre for Polar and Marine Research, 27568 Bremerhaven, Germany
[4]Faculty of Geosciences (FB5) and Center for Marine Environmental Sciences (MARUM), University of Bremen, 28359 Bremen, Germany
[5]Key Laboratory of Marine Chemistry Theory and Technology, Ocean University of China, 266100 Qingdao, China

10   *Correspondence to*: Wanyee Wong (yunw@norceresearch.no)

Abstract. To better understand the processes in the Nordic Seas and their connection to large-scale climate changes during Dansgaard-Oeschger (D-O) events, we reconstruct sea ice extent (SIE) and subsurface temperatures (SubSTs) in the eastern Fram Strait between 40 and 33.5 ka b2k. Our new proxy data from MD99-2304 reveal pronounced fluctuations in SIE and
15   SubSTs both between and within each investigated Greenland Stadial (GS) and Greenland Interstadials (GIs). Consequently, variations in SIE and SubSTs in the eastern Fram Strait show a weaker connection to climate oscillations in Greenland ice cores, in comparison to changes observed in the southeastern Nordic Seas and the North Atlantic.

Integrating our results with AMOC strength reconstructions and sea ice records from the southeastern Nordic Seas, we identify different sea ice regimes between the eastern Fram Strait and the southeastern Nordic Seas. These findings suggest
20   that fluctuations in the eastern Fram Strait were primarily driven by shifts in northward oceanic heat transport, which were regulated by changes in the strength of the Atlantic Meridional Overturning Circulation (AMOC).

1 Introduction

A series of rapid climate oscillations known as the Dansgaard-Oeschger (D-O) events characterized Marine Isotope Stage (MIS) 3 (Dansgaard et al., 1982; North Greenland Ice Core Project members, 2004). Each D-O event featured an abrupt
25   warming to a mild Greenland Interstadial (GI) state and then a gradual cooling to a glacial Greenland Stadial (GS) state. These shifts were considered repeated oscillations based on Greenland ice core $\delta^{18}O$ records (Mogensen, 2009; Rasmussen et al., 2014). While the duration of the events as seen in Greenland $\delta^{18}O$ records differed and deviations in their appearance existed, the succession of events and types of signals within the GSs and GIs were comparable (Rasmussen et al., 2014).

Several paleoenvironmental reconstructions and modeling studies have suggested that the sea ice extent (SIE) in the Nordic
30   Seas experienced consistent phase shifts during the D-O events, with an extensive sea ice cover during GSs and seasonal sea

ice cover during GIs (e.g., Dokken et al., 2013; Hoff et al., 2016; Sadatzki et al., 2019, 2020; Pedro et al., 2022; El bani Altuna et al., 2024). In the Faroe-Shetland Channel, SIE reductions consistently occurred before Greenland warming, while its expansion preceded Greenland cooling. These on/off SIE signals were observed consistently for all D-O events between 30 and 40 ka b2k (Sadatzki et al., 2019, 2020). Such shifts in SIE were proposed to have contributed to the D-O climate

35   oscillations through their impact on ocean-ice-atmosphere interactions (Li and Born, 2019; Pedro et al., 2022). In the northernmost Nordic Seas, specifically the Fram Strait, constant sea ice coverage occurred throughout both GSs and GIs (El bani Altuna et al., 2024). Based on analyses of a series of idealized model experiments, Buizert et al. (2024) argued that the North Atlantic sea ice cover was more critical than that of the Nordic Seas for influencing the D-O signal as seen in the Greenland ice cores.

40   These past studies presented a consistent picture of the relationship between Nordic Seas SIE and Greenland climate records, with a steadily repetitive pattern of variability through the course of the D-O events. However, a recent study by Wong et al. (2024) showed that polynyas were present in the eastern Fram Strait through much of HS-4 (also known as GS-9). The presence of polynyas indicated that parts of the northernmost Nordic Seas experienced ice-free conditions, contrasting with previous studies that argued for a perennial sea ice cover north of the Vøring Plateau (Sadatzki et al., 2020; El bani Altuna et

45   al., 2024). This polynya activity was suggested to be a response to ocean sensible heat flux (Wong et al., 2024). Wong et al. (2024) also showed that the seasonal sea ice cover retreated to the eastern Fram Strait during GI-8, documenting that there were more ice-free areas in the Nordic Seas during GI-8 than formerly proposed (Sadatzki et al., 2019, 2020; El bani Altuna et al., 2024).

The results from Wong et al. (2024) suggested that sea ice in the northernmost Nordic Seas may have behaved differently

50   during GSs and GIs than previously thought. However, it remains unknown whether polynya activity was a regularly occurring phenomenon in the northernmost Nordic Seas also during other stadials, or if it was limited to HS-4.

Previous studies investigating changes in the Atlantic Meridional Overturning Circulation (AMOC) (Henry et al., 2016) and Southern Ocean ventilation (Yu et al., 2023) suggested that ocean circulation behavior was not consistent across GSs. This contrasted with the commonly held perspective that climate variability during this period followed a consistently repeating

55   pattern, as observed in Greenland.

Ocean heat transport and SIE are closely interconnected (e.g., Mahajan et al., 2011; Day et al., 2012; Polyakov et al., 2017; Årthun et al., 2019). Moreover, the heat-laden Atlantic Water (AW) inflow into the Nordic Seas is suggested to be related to the strength of the AMOC (Larson et al., 2020). Therefore, it is reasonable to expect that the varying ocean circulation strength observed during D-O events influenced ocean temperatures as well as SIE in the Nordic Seas. Here we will

60   investigate how the SIE and sea subsurface temperatures (SubSTs) in the Nordic Seas changed through GS-9 to GS-7 (39.9–33.74 ka b2k, thousand years before the year 2000), and whether and how these changes may have been driven by changes in the AMOC (Henry et al., 2016).

To do so, we reconstruct the northernmost Nordic Seas SIE semi-quantitively with lipid biomarker proxies and indices, including the highly branched isoprenoids (HBIs) IP_{25} and HBI-III (Z), sterols brassicasterol and dinosterol, and PIP_{25}

65   indices from marine sediment core MD99-2304 in the eastern Fram Strait (1348 m water depth; 77°37'15.6"N 9°56'54"E)
(Fig. 1). We also reconstruct the SubSTs based on Mg/Ca. To evaluate the relationship between ocean circulation changes
and sea ice, our new records from the northernmost Nordic Seas are compared with sea ice reconstructions from other parts
of the eastern Nordic Seas (Sadatzki et al., 2019, 2020; El bani Altuna et al., 2024) and AMOC reconstructions from the
North Atlantic (Henry et al., 2016).

70
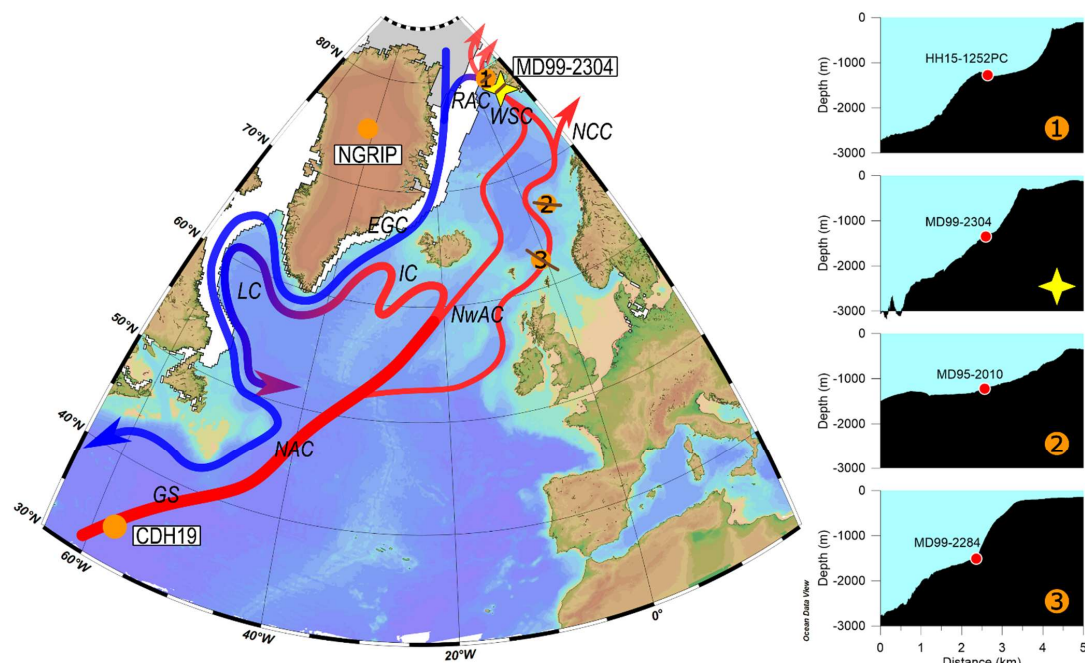
Figure 1. Map of the research area with modern-day conditions (updated from Wong et al. 2024). Core MD99-2304 is highlighted
with a light-yellow star. For a comprehensive understanding of SIE across different periods, we compare our results with
biomarker data from (1) HH15-1252PC (El bani Altuna et al., 2024), (2) MD95-2010 (Sadatzki et al., 2020), (3) MD99-2284 (Sadatzki
et al., 2019), and Pa/Th record from CDH19 (Henry et al., 2016). The 2024 September SIE and 2025 March SIE are marked with
75   gray and white areas, respectively (Florence et al., 2017, updated to 2025). The Gulf Stream (GS), North Atlantic Current (NAC),
Irminger Current (IC), Norwegian Atlantic Current (NwAC), North Cape Current (NCC), and West Spitzbergen Current (WSC)
are illustrated with red arrows, while the East Greenland Current (EGC) and Labrador Current (LC) are depicted by blue or red-
blue arrows. Between the WSC and EGC, the Return Atlantic Current (RAC) at intermediate water depth is shown as a red-blue
line. The right panel displays the cross profile of each site in the eastern Nordic Seas, indicated by brown lines in the map. The
80   basemap was created using Ocean Data View (https://odv.awi.de/), based on the World Ocean Database. Currents and sites are
added using Inkscape (http://www.inkscape.org/).

2 Present-day oceanography

The Fram Strait is the northernmost part of the Nordic Seas and one of the main passages where the warm and saline Atlantic
85 Water (AW) enters the Arctic Ocean at intermediate water depths (Smedsrud et al., 2022). The North Atlantic Current
(NAC) originates in the Gulf Stream (GS) (Orvik and Niiler, 2002) and travels northward and then eastward across the
Atlantic Ocean. It splits into the two-branched Norwegian Atlantic Current (NwAC) and the Irminger Current (IC)
(Blindheim and Østerhus, 2005; Bosse et al., 2018). Both branches of the NwAC enter the Nordic Seas over the Greenland-
Scotland Ridge. The eastern branch flows along the Norwegian continental slope (Poulain et al., 1996; Bosse et al., 2018).
90 The eastern branch of the NwAC bifurcates in the northern Norwegian Sea, from where the North Cape Current (NCC)
flows into the Barents Sea (Ingvaldsen, 2005). The West Spitsbergen Current (WSC), merged with the western branch of the
NwAC, flows into the eastern Fram Strait (Furevik, 2001; Bosse et al., 2018) (Fig. 1).

The AW is gradually densified due to ocean heat loss during the northward transport. In the eastern Fram Strait, the densified
AW submerges, before entering the Arctic Ocean over the Yermak Plateau or turning southwards, through the Return
95 Atlantic Current (RAC), at intermediate depths (Gordon, 1986; Hattermann et al., 2016). Above the RAC, cold and fresh
Polar Water (PW) is transported southwards through the East Greenland Current (EGC) along the Greenland continental
margin (Fahrbach et al., 2001). Across the Demark Strait, the EGC interacts with the recirculated IC (Holliday et al., 2007).
These currents feed into the boundary current in the Labrador Sea, known as the Labrador Current (LC) (Cuny et al., 2002)
(Fig. 1).
100 This current system, which transports multiple water masses across these Northern Seas, is a crucial component of the
AMOC (Bryden, 2021). The poleward AW brings heat and salt to high latitudes. The recirculated, densified AW in the
Nordic Seas contributes to the formation of North Atlantic Deep Water (NADW) (Hall and Bryden, 1982; Petit et al., 2021).
Variations in this ocean circulation system have a great impact on large-scale climate patterns, including sea ice conditions,
ocean heat content distribution, atmospheric temperature, and wind patterns (Liu et al., 2017; Årthun et al., 2019; Lozier et
105 al., 2019). The topographic features of the seabed in the Nordic Seas create constraints for incoming water masses,
influencing their properties, distribution, and interactions. On a large scale, these features affect the dynamics of ocean
currents, shaping the overall circulation patterns in the region (Blindheim and Østerhus, 2005). In the northern Nordic Seas,
the narrowing passage constricts the inflow, triggering internal wave breakup and vertical mixing. This process, in turn,
influences the thermal structure as the AW continues its northward journey (e.g., Falk-Petersen et al., 2015; Bensi et al.,
110 2019; Zhang et al., 2022) (Fig. 1).

3 Methodology

3.1 Chronological framework

The chronology of MD99-2304 was presented in Wong et al. (2024), based on tuning the low field magnetic susceptibility (Klf) of MD99-2304 to the Klf of the core MD95-2010 from the central Norwegian Sea (2 in Fig. 1) (Kissel et al., 1999).

115 The age-depth model of MD95-2010 was tied to the chronology of MD99-2284 from the Faeroe-Shetland Channel, an age model linked to Greenland through identification of microtephra layers (Berben et al., 2020; Sadatzki et al., 2020). All ages are given as thousand years before the year 2000 (ka b2k).

3.2 Biomarker analysis

Core MD99-2304 was analyzed every 0.5–1 cm (ca. 20–40 years/sample) between 813.25 and 974.75 cm (ca. 40–33.7 ka

120 b2k). Biomarkers were measured in 248 samples. The 149 samples focusing on the HS-4 and GI-8 (ca. 40–36.5 ka b2k, 874.25–974.25 cm) were presented and discussed in Wong et al. (2024). All samples were freeze-dried and homogenized. For biomarker concentration normalization, total organic carbon (TOC) was measured with 90 mg of sediment using a Carbon-Sulfur Analyzer (CS-125, Leco), after the carbonate in sediments was removed with hydrochloric acid (HCl) of 20% solution.

125 The internal standards 7-hexylnonadecane (7-HND, 0.066 µg, for IP$_{25}$ quantification), 9-octylheptadec-8-ene (9-OHD, 0.1 µg, for different quality control procedures), 5α-androstan-3β-ol (androstanol, 10.6 µg, for sterols), and 2,6,10,15,19,23-hexamethyltetracosane (squalane, 3.2 µg, for n-alkanes if needed later) were added to each sample prior to extraction. The total lipid extracts (TLEs) were extracted by ultrasonication for 15 min and centrifugation (2000 rpm) for 3 min, using dichloromethane:methanol (2:1, v/v) as a solvent, and the procedure was repeated three times. Then the TLEs were separated

130 using open silica (SiO2) column chromatography, with n-hexane (5 ml) and ethyl acetate:n-hexane (9 ml, 2:8 v/v) as eluent into the hydrocarbon and sterol fractions. The sterol fraction was silylated using 200 µl bis-trimethylsilyl-trifluoroacet-amide (BSTFA) at 60 °C for 2 h. The biomarkers were measured by gas chromatography/mass spectrometry (GC/MS) using an Agilent 7890B GC (30m DB-1MS column, 0.25 mm i.d., 0.25 µm film thickness) coupled to an Agilent 5977A mass selective detector (MSD, 70 eV constant ionization potential, Scan 50–550 m/z, 1 scan/s, ion source temperature 230°C,

135 Performance Turbo Pump). Ion monitoring mode (SIM) was selected for HBIs and full scan mode (50-550 m/Z) for sterols. We focus on two highly branched isoprenoids (HBIs), IP$_{25}$ and HBI-III (Z), and two sterols, brassicasterol and dinosterol. The selected biomarkers were identified based on their GC retention times in comparison to those of specific reference compounds as well as published mass spectra for HBIs (Belt et al., 2000, 2007) and for sterols (Boon et al., 1979; Volkman, 1986). HBIs were quantified based on their molecular ions, m/z 350 for IP$_{25}$ and m/z 346 HBI-III (Z), in relation to the

140 fragment ion m/z 266 of 7-HND. Brassicasterol and dinosterol were quantified with molecular ions m/z 470, 500, 472, and 486, respectively, in relation to the molecular ion m/z 348 of androstanol (Wong et al., 2024). An external calibration was applied, to balance different responses of molecular ions of the analytes and the molecular/fragment ions of the internal

standards (Fahl and Stein, 2012). All analyses were performed at the Alfred Wegener Institute (AWI) Bremerhaven, Germany.

145 Since IP$_{25}$ cannot be interpreted for SIE solely (Müller et al., 2011; Stein et al., 2017; Köseoğlu et al., 2018; Kolling et al., 2020), all biomarkers are interpreted combined. PIP$_{25}$ (open water phytoplankton biomarker-IP$_{25}$ index) indices are introduced to differentiate between perennial sea ice cover and open ocean (Müller et al., 2011). For detailed calibrations of PIP$_{25}$ indices, please refer to Wong et al. (2024).

Based on the intercomparison between marine sediment biomarker records and modern SIE observations, sea ice conditions
150 are defined into four types. When PIP$_{25}$ values are lower than 0.1, it refers to ice-free conditions. PIP$_{25}$ values between 0.1 and 0.5 are defined as limited level of sea ice. 0.5–0.75 in PIP$_{25}$ values mean seasonal sea ice. When PIP$_{25}$ values are higher than 0.75, an extensive to nearly perennial sea ice cover is defined (Müller et al., 2011; Xiao et al., 2015; Stein et al., 2017).

3.3 Planktonic foraminifera Mg/Ca measurement

Neogloboquadrina pachyderma was dry-sieved between 150 to 212 μm and handpicked every 0.5–1.5 cm between 813.25
155 and 946.5 cm. The final resolution is a result of availability of foraminifera in the samples. Trace element analysis was carried out on approximatively 100 crushed foraminiferal shells per sample after a "full cleaning" protocol (Boyle, 1981; Boyle and Keigwin, 1985). This protocol includes clay, metal oxides and barite removal steps, oxidation of the organic matter and surface leaching. The analysis was run at the Trace Element Lab (TELab) at NORCE Bergen, Norway on an Agilent 720 inductively coupled plasma optical emission spectrometer (ICP-OES). Measured N. pachyderma Mg/Ca
160 (Mg/Ca$_{N.p}$) ratios showed negligible correlation with Fe/Ca, Al/Ca and Mn/Ca ratios, with r^2 values of 0.003, 0.0067, 0.002 respectively, indicating no contamination due to an insufficient cleaning. Long-term precision based on carbonate standard ECRM-752-1 yielded to 3.76 mmol.mol-1 (1s = 0.007 mmol.mol-1). Mg/Ca$_{N.p}$ values were then calibrated to SubSTs via the following equation according to Elderfield and Ganssen (2000):

$$T = 10 * \ln \left((Mg/Ca_{N.p})/0.52 \right)$$

165 We also tested SubST calibration equations for Mg/Ca$_{N.p}$ following Morley et al. (2024) which employed "Mg cleaning" (Barker et al., 2003) and Ezat et al. (2016) which used "full cleaning" (Boyle and Keigwin, 1985; Martin and Lea, 2002; Barker et al., 2003). However, the resulting SubSTs were generally 5–10°C, which we considered unrealistically high for high-latitude oceans during the glacial period. Temperatures in the range of 5–10°C should have been reflected in the planktic foraminiferal fauna through reduced relative abundance of N. pachyderma, even at the fraction >150μm. However,
170 with very few exceptions, there was more than 94% N. pachyderma in the samples (data not shown), indicating temperatures less than 6°C (Govin et al., 2012). Therefore, we proceeded with the calibration equation from Elderfield and Ganssen (2000).

4 Results

4.1 Greenland Stadials

175   The proxy records from the eastern Fram Strait reveal that the intra-GS SIE and SubST developments differed between each investigated GS. Among the three studied GSs (HS-4, GS-8, and GS-7), HS-4 shows the highest and most frequent variability in biomarker concentrations and PIP_{25} indices. The maximum and minimum values for both biomarker concentrations and PIP_{25} indices are observed during HS-4, with all changes occurring abruptly (Wong et al., 2024). The SubSTs reconstructed based on $Mg/Ca_{N.p}$ only cover the period starting from 39.3 ka b2k. Following the low values around

180   0–3°C between 39.4 and 39.1 ka b2k, the SubSTs remained relatively stable at around 2–4°C for the rest of HS-4.

In contrast to HS-4, biomarker concentrations and PIP_{25} indices during GS-8 show clear trends with few fluctuations. IP_{25} concentrations increased from low values, while brassicasterol concentrations decreased from high values following the end of the preceding GI-8. HBI-III (Z) and dinosterol concentrations remained stable. These trends lead to PIP_{25} indices increasing almost steadily from ca. 0.3 to 0.7 throughout GS-8. SubSTs varied between 1°C and 4°C during GS-8, with

185   much sharper changes and more low values compared to HS-4.

The conditions during GS-7 were less variable than those in the other two GSs. IP_{25} concentrations were overall high, while phytoplankton biomarker concentrations remained stably low. PIP_{25} indices stayed constant at ca. 0.6. Most of the SubSTs during GS-7 were around 3–6°C, with the higher values seen early in GS-7 (Fig. 2).
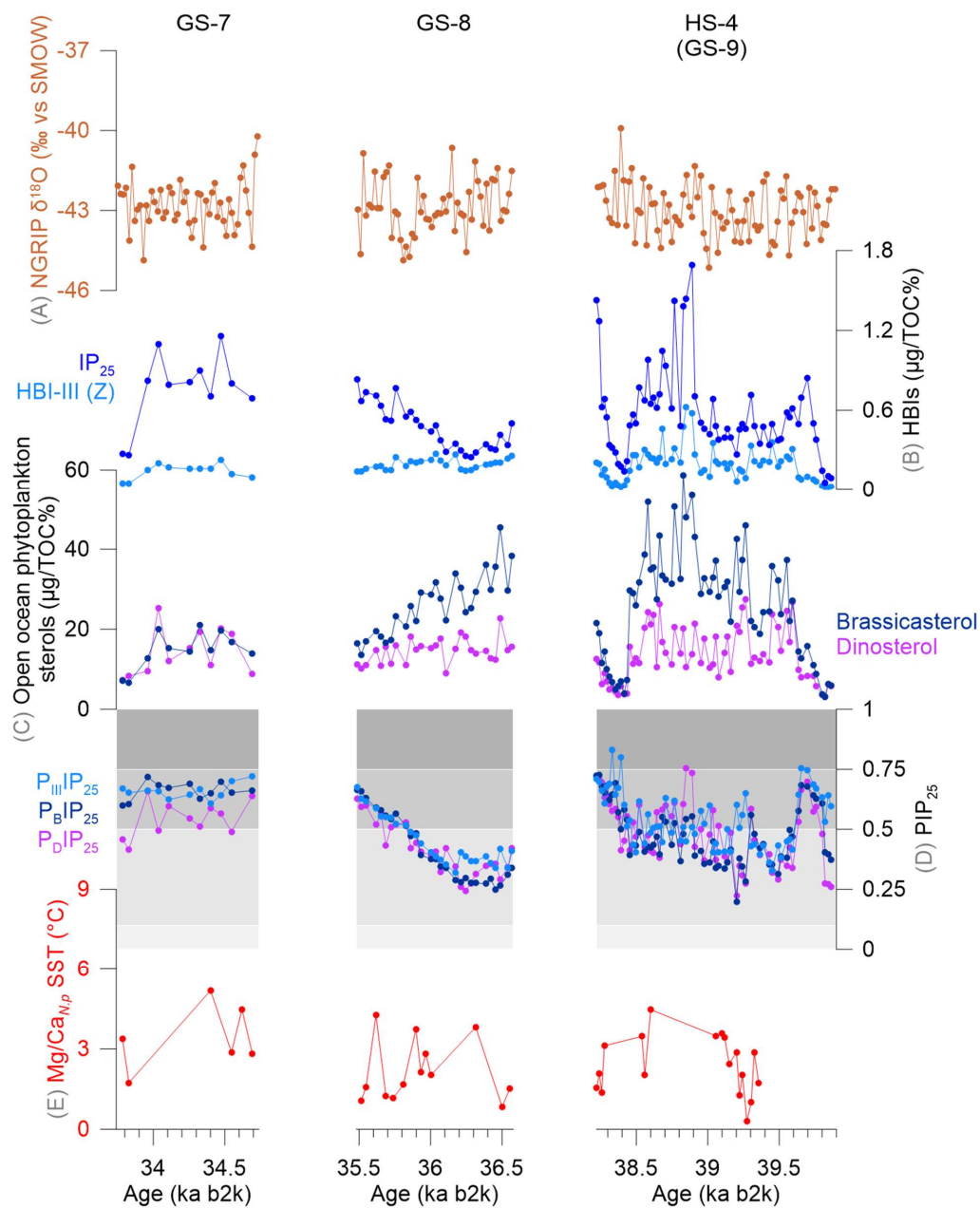
190 **Figure 2. Comparison of biomarker results from MD99-2304 across HS-4, GS-8, and GS-7. (A) NGRIP δ^{18}O** (North Greenland Ice Core Project members, 2004; Andersen et al., 2006)**, (B) IP$_{25}$ and HBI-III (Z), (C) brassicasterol and dinosterol, (D) PIP$_{25}$, and (E) SubST reconstruction from Mg/Ca$_{N.p}$. The pink bars indicate GIs as defined in the NGRIP ice core** (Rasmussen et al., 2014)**. The boxes in the PIP$_{25}$ indices** stand for categories **of sea ice conditions (from darkest to lightest grey: 0.75–1 extensive sea ice, 0.5–0.75 seasonal ice / stable ice edge, 0.1–0.5 little but variable ice extent, 0–0.1 ice-free)** (Xiao et al., 2015; Stein et al., 2017)**.**

195 **4.2 Greenland Interstadials**

As seen for the GSs, proxy records from the eastern Fram Strait indicate that the development, amplitude, and frequency of variations differed both within individual GIs and among different GIs. Both the investigated GIs (GI-8 and GI-7) can be divided into two periods based on changes in biomarker concentrations and PIP$_{25}$ indices. However, the patterns within each period are not comparable. The highest and most variable HBI concentrations occurred during the first half of GI-8, while

200 sterol concentrations became more variable during the second half of GI-8. This results in higher but fluctuating PIP$_{25}$ indices in the first half of GI-8, followed by more stable yet lower PIP$_{25}$ indices in the second half (Wong et al., 2024). SubSTs during GI-8 are reconstructed at a low temporal resolution due to the scarcity of planktonic foraminifera. The available data indicates low SubSTs around 0–3°C at the onset of GI-8, while the temperatures varied between 3°C and 6°C otherwise (Fig. 3).

205 In contrast to GI-8, PIP$_{25}$ indices present a decline during the first half of GI-7 and a shift toward higher values in the second half. Overall, PIP$_{25}$ indices were in general higher during GI-7 than in GI-8. This is due to differences in biomarker concentrations. IP$_{25}$ concentrations decreased and remained low during the first half of GI-7, followed by an increase in the second half. HBI-III (Z) concentrations were slightly higher initially but then decreased slowly during both halves of GI-7. Although sterol concentrations remained generally low throughout GI-7, they also display a two-phase pattern, with an initial

210 increase in the first half succeeded by a gradual decrease in the second half. Moreover, SubSTs exhibit a similar two-phase trend to that of the biomarker concentrations, first increasing and then decreasing, with a turning point occurring at mid-GI-7 (35.1 ka b2k) (Fig. 3).
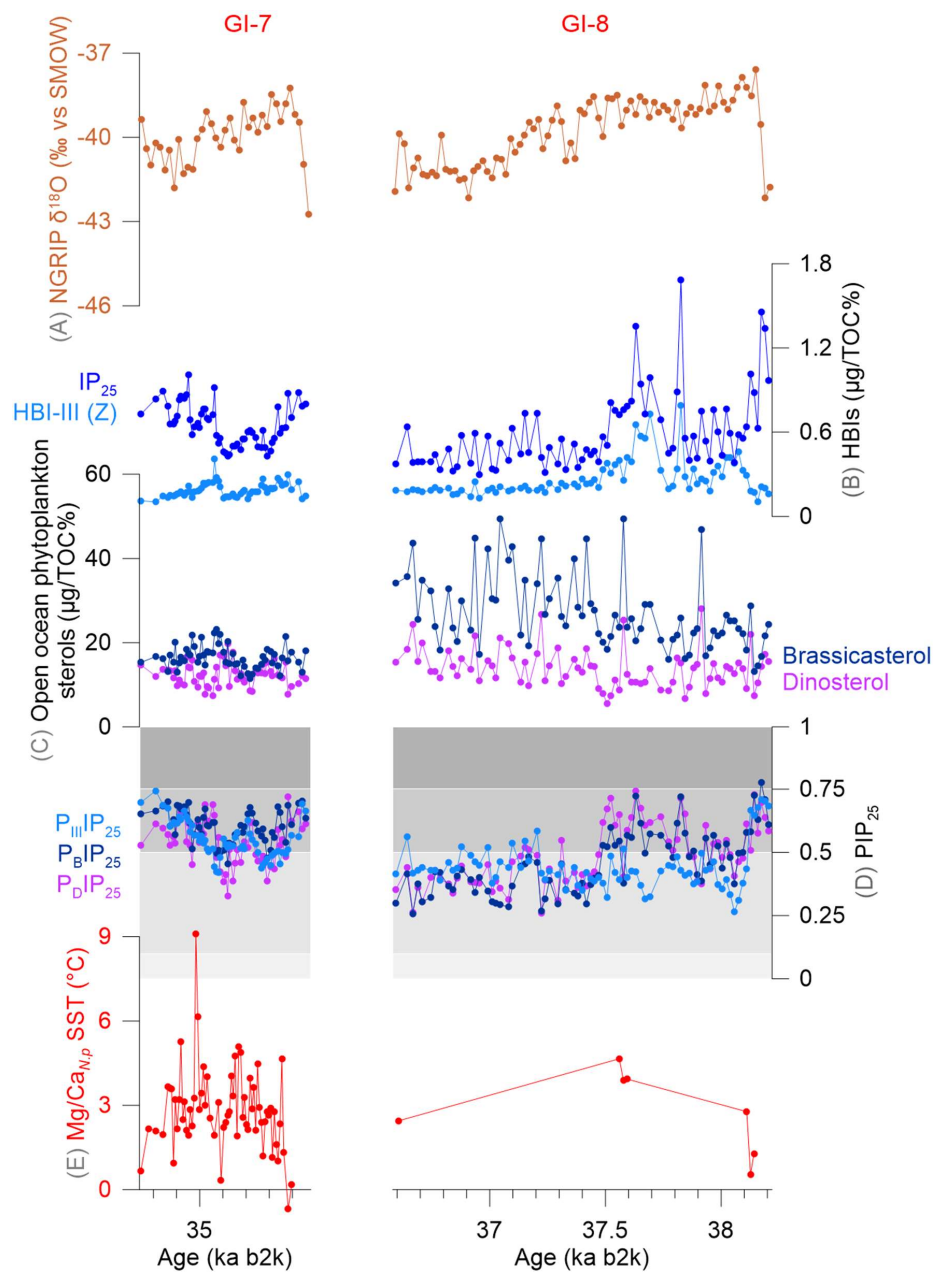
Figure 3. Comparison of biomarker results from MD99-2304 across HS-4, GS-8, and GS-7. (A) NGRIP δ¹⁸O (North Greenland Ice
Core Project members, 2004; Andersen et al., 2006)**, (B) IP$_{25}$ and HBI-III (Z), (C) brassicasterol and dinosterol, (D) PIP$_{25}$, and (E)
SubST reconstruction from Mg/Ca$_{N,p}$. The boxes in the PIP$_{25}$ indices stand for categories of sea ice conditions (from darkest to
lightest grey: 0.75–1 extensive sea ice, 0.5–0.75 seasonal ice / stable ice edge, 0.1–0.5 little but variable ice extent, 0–0.1 ice-free)**
(Xiao et al., 2015; Stein et al., 2017)**.**

5 Discussion

The new proxy-based reconstruction from MD99-2304 show that the SIE and SubSTs varied between each GS in the eastern
Fram Strait. In the same way, the progression of SIE and SubSTs differed between the investigated GIs (Fig. 4). Within
individual GSs and GIs, SIE and SubSTs were also less stable than previously assumed (Fig. 4). When considered alongside
existing sea ice records from an eastern Nordic Seas transect (Sadatzki et al., 2019, 2020; El bani Altuna et al., 2024), our
SIE and SubST reconstructions highlight the distinctly different sea ice conditions in the northernmost Nordic Seas. These
findings reveal that glacial sea ice conditions in the eastern Fram Strait differed from those in the southeastern Nordic Seas
(Fig. 4).
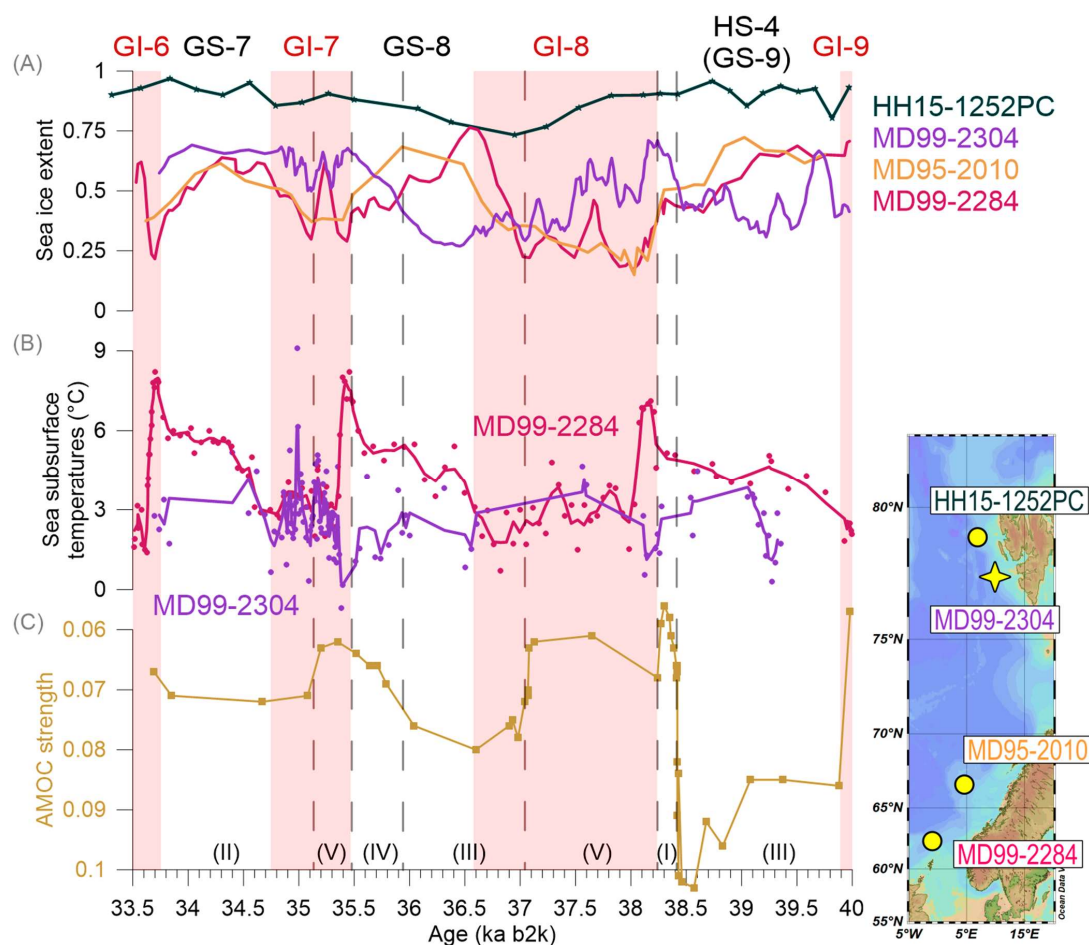
Figure 4. Comparison of sea surface and subsurface conditions between the southeastern and northern Nordic Seas. (A) Sea ice extent (SIE) reconstructions from HH15-1252PC ($P_{III}IP_{25}$; El bani Altuna et al., 2024)**, MD99-2284 (P_BIP_{25} smoothed;** Sadatzki et al., 2019)**, MD95-2010 (P_BIP_{25} smoothed;** Sadatzki et al., 2020)**, and MD99-2304 (P_BIP_{25} smoothed). (B) Sea subsurface temperatures (SubSTs) from MD99-2284 (smoothed, estimated using the maximum likelihood transfer function on planktic foraminifera census counts;** Dokken et al., 2013 and Sadatzki et al., 2019) **and MD99-2304 (smoothed, based on Mg/Ca$_{N.p}$). The sites are illustrated on the map in the right corner using Ocean Data View (https://odv.awi.de). The SIE and SubST datasets are compared with (C) AMOC strength records (based on Pa/Th) from the Bermuda Rise (Core CDH19)** (Henry et al., 2016)**. Modes I to V are separated by grey dashed lines and labeled in parentheses. All smoothed lines are derived using a 3-point moving average. The original SubST data are marked with red round symbols.**

5.1 Modes of variability

We hypothesize that shifts in oceanic heat distribution driven by variations in large-scale ocean circulation, regulated SIE and SubSTs in the eastern Nordic Seas during the investigated period. One of the key drivers of modern Arctic SIE variations is the large-scale ocean circulation and heat transport (e.g., Polyakov et al., 2017; Docquier and Koenigk, 2021; Docquier et al., 2022). Anomalies in ocean heat transport into the Nordic Seas originate in the subpolar North Atlantic (Årthun and Eldevik, 2016), with the AMOC and the subpolar gyre (SPG) component contributing equally to the heat transport when crossing the Greenland-Scotland Ridge (Rhein et al., 2011; Li and Born, 2019).

However, due to the lack of SPG component reconstructions, we use the existing AMOC reconstruction (Fig. 4C) (Henry et al., 2016) as a proxy for ocean heat transport to the Nordic Seas. Modeling studies (Sun et al., 2021; Jones et al., 2024), observational data (Mandal et al., 2024) and combined approaches (Rhein et al., 2011) indicate that SPG and AMOC strengths are correlated on multidecadal timescales. Therefore, in this study, we assume that ocean heat transport into the Nordic Seas is linked to the strength of the AMOC (Day et al., 2012; Årthun et al., 2019; van der Linden et al., 2019). Based on SIE and SubSTs from MD99-2304 and previously published sites in the southeastern Nordic Seas (Sadatzki et al., 2019, 2020), complemented by the Pa/Th-based AMOC reconstruction by Henry et al. (2016), we define five modes of variability that characterize the observed dynamic interplay between ocean circulation, ocean temperatures, and sea ice conditions (Figs. 4 & 5). Sedimentary Pa/Th is considered a proxy for past ocean circulation strength (e.g., Bradtmiller et al., 2014; Robinson et al., 2019; Missiaen et al., 2020). In this study, we use Pa/Th values of <0.065, 0.065–0.075, and >0.075 to correspond to strong, intermediate, and weak AMOC strengths, respectively.
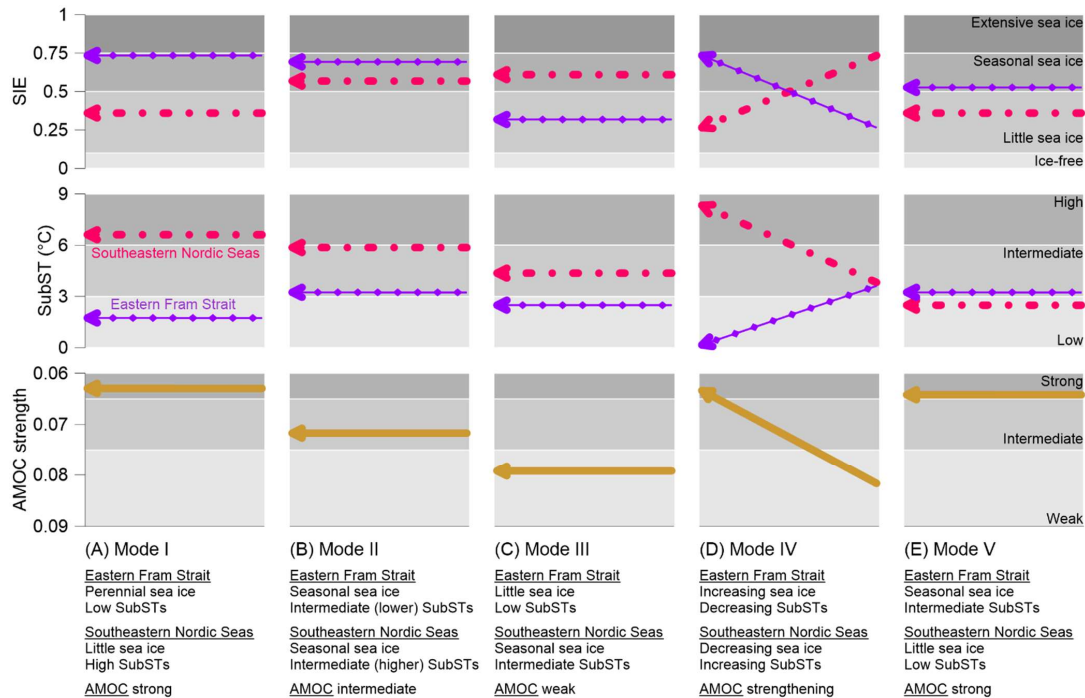
Figure 5. Schematic illustration of the relationships between AMOC strength and the eastern Nordic Seas SIE and SubSTs. Five modes are identified: (A) Mode I, (B) Mode II, (C) Mode III, (D) Mode IV, and (E) Mode V. The purple lines with diamonds represent records from MD99-2304 in the eastern Fram Strait, and the magenta dashed lines represent records from MD99-2284 and MD95-2010 in the southeastern Nordic Seas. The boxes in the PIP$_{25}$ indices stand for categories of sea ice conditions (from darkest to lightest grey: 0.75–1 extensive sea ice, 0.5–0.75 seasonal ice / stable ice edge, 0.1–0.5 little but variable ice extent, 0–0.1 ice-free) (Xiao et al., 2015; Stein et al., 2017)**. SubSTs are classified into three categories: high (>6°C, dark grey box), intermediate (3–6°C, medium grey box), and low (<3°C, light grey box). AMOC strength is inferred from Pa/Th values. Pa/Th <0.065 is considered to indicate strong AMOC (dark grey box), 0.065–0.075 intermediate AMOC (medium grey box), and >0.075 weak AMOC (lightest grey box).**

5.1.1 Mode I

==Mode I== (Fig. 5A) is characterized by a perennial sea ice cover (Wong et al., 2024) and low SubSTs in the eastern Fram Strait, corresponding with little SIE and high SubSTs in the southeastern Nordic Seas (Sadatzki et al., 2019, 2020). Meanwhile, the AMOC was strong (Figs. 4 & 5A).

The presence of perennial sea ice in the eastern Fram Strait is documented by low biomarker concentrations from MD99-2304. Although PIP$_{25}$ indices are high, they still underestimate SIE due to these low biomarker concentrations (Fig. 2)

(Wong et al., 2024). Biomarker records from HH15-1252PC, located northwest of MD99-2304 in the northeastern Fram Strait, also indicate perennial sea ice (El bani Altuna et al., 2024). However, little SIE is observed in the southeastern Nordic Seas (MD95-2010 and MD99-2284) (Sadatzki et al., 2019, 2020) (Fig. 4A). Differences in temperature reconstructions further support these sea ice patterns. Low SubSTs in the eastern Fram Strait are suggested by low temporal resolution
275   Mg/Ca-based temperature reconstructions (Mg/Ca$_{N,p}$). In the southeastern Nordic Seas (MD99-2284), a foraminiferal transfer function-based temperature reconstruction presents high SubSTs (Sadatzki et al., 2019) (Fig. 4B). The AMOC is defined to be strong, based on a Pa/Th value <0.065 (Figs. 4C & 5A).

5.1.2 Mode II

Mode II (Fig. 5B) represents periods when seasonal sea ice dominated both the eastern Fram Strait and the southeastern
280   Nordic Seas. SubSTs were at intermediate levels in both the north and south (Sadatzki et al., 2019, 2020). SIE and SubSTs show reduced contrasts between the north and south compared to Mode I (Fig. 5A & B). During this mode, the AMOC remained at an intermediate strength (Figs. 4 & 5B).

The Mode II seasonal, nearly extensive sea ice in the eastern Fram Strait is supported by high IP$_{25}$, low HBI-III (Z), low sterol concentrations, and high PIP$_{25}$ indices (Stein et al., 2017; Köseoğlu et al., 2018) (Figs. 2 & 3). Perennial sea ice
285   persisted at HH15-1252PC (El bani Altuna et al., 2024). Further south, seasonal sea ice expanded into the southeastern Nordic Seas (Sadatzki et al., 2019, 2020) (Fig. 4A). Temperature reconstructions suggest intermediate Mg/Ca$_{N,p}$-based SubSTs in the eastern Fram Strait (MD99-2304), though the lack of continuous data prevents a more precise interpretation. In the southeastern Nordic Seas (MD99-2284), foraminiferal transfer function-based SubSTs were also at intermediate levels but remained higher than those from the eastern Fram Strait during this mode (Sadatzki et al., 2019) (Fig. 4B). The AMOC
290   was at intermediate strength, with Pa/Th values between 0.065 and 0.075 (Figs. 4C & 5B).

5.1.3 Mode III

Mode III (Fig. 5C) features little SIE and low SubSTs in the eastern Fram Strait (Wong et al., 2024), while the southeastern Nordic Seas experienced seasonal sea ice and intermediate SubSTs (Sadatzki et al., 2019, 2020). The AMOC was weak during this mode (Figs. 4 & 5C).

295   In the eastern Fram Strait, nearly ice-free conditions are reflected by varying HBI, high sterol concentrations, and consistently low PIP$_{25}$ indices from MD99-2304 (Stein et al., 2017; Köseoğlu et al., 2018) (Figs. 2 & 3). This evidence points to repeated polynya activity (Wong et al., 2024), since perennial sea ice was suggested to have covered the Vøring Plateau and areas to its north (Sadatzki et al., 2019, 2020). However, the polynyas at MD99-2304 were likely small and local in extent since the biomarker records from the nearby HH15-1252PC document persistent perennial sea ice (Fig. 4A) (El
300   bani Altuna et al., 2024). Meanwhile, Mg/Ca$_{N,p}$-based SubSTs remained low in the eastern Fram Strait, while foraminiferal transfer function-based SubSTs reached intermediate levels in the southeastern Nordic Seas (Sadatzki et al., 2019) (Fig. 4B). During this mode, based on Pa/Th values >0.075, the AMOC is classified as weak (Figs. 4C & 5C).

5.1.4 Mode IV

Mode IV (Fig. 5D) displays a trend of increasing SIE and decreasing SubSTs in the eastern Fram Strait, following Mode III

305 when polynyas were present. In contrast, in the southeastern Nordic Seas, SIE decreased and SubSTs increased (Sadatzki et al., 2019, 2020). During this mode, the AMOC continued to strengthen (Figs. 4 & 5D).

Starting with nearly ice-free conditions, the eastern Fram Strait saw a rise in SIE, as indicated by increasing IP_{25} and decreasing sterol concentrations, along with increasing PIP_{25} values (Stein et al., 2017; Köseoğlu et al., 2018) (Figs. 2 & 4). In the meantime, a perennial sea ice cover dominated at HH15-1252PC (El bani Altuna et al., 2024). In contrast, biomarker

310 records from the southeastern Nordic Seas show an opposite trend, with SIE continuously decreasing (Sadatzki et al., 2019, 2020) (Figs. 4A). $Mg/Ca_{N.p}$-based SubSTs gradually decreased in the eastern Fram Strait, while foraminiferal transfer function-based SubSTs continued to rise in the southeastern Nordic Seas (Sadatzki et al., 2019) (Fig. 4B). The AMOC is observed strengthening, with Pa/Th values decreasing from >0.075 to <0.065 (Figs/ 4C & 5D).

5.1.5 Mode V

315 Mode V (Fig. 5E) is marked by seasonal sea ice and intermediate SubSTs in the eastern Fram Strait, and little SIE with low SubSTs in the southeastern Nordic Seas (Sadatzki et al., 2019, 2020). The AMOC strength was similar to that of Mode I (Figs. 4 & 5E).

Low HBI, high sterol concentrations and low PIP_{25} indices at MD99-2304 suggest the presence of seasonal sea ice (Stein et al., 2017; Köseoğlu et al., 2018). Conversely, biomarker evidence from HH15-1252PC in the northeastern Fram Strait

320 indicates an extensive sea ice cover (Fig. 4A) (El bani Altuna et al., 2024), pointing to a sea ice margin between the two core sites. In the southeastern Nordic Seas, biomarker records indicate nearly ice-free conditions (Sadatzki et al., 2019, 2020) (Fig. 4A). $Mg/Ca_{N.p}$-based SubSTs at MD99-2304 averaged slightly above 3°C, the boundary between intermediate and low levels defined in this study. Foraminiferal transfer function-based SubSTs were slightly lower than 3°C at MD99-2284 (Sadatzki et al., 2019) (Fig. 4B). The AMOC was strong, comparable to Mode I (Pa/Th <0.065).

325 Combined, these findings imply a substantial seasonally ice-free area along the eastern Nordic Seas, extending into the eastern Fram Strait. Among all five modes, this one is the most similar to present-day conditions.

5.2 Mechanistic description of the modes

Of the identified modes of variability outlined in Section 5.1, Modes I and IV occurred during GSs, Mode V occurred during GIs, and Modes II and III occurred during both GSs and GIs. We argue that the interaction between surface and subsurface

330 ocean heat content in the southeastern Nordic Seas, influenced by the state of the AMOC, played a key role in shaping sea ice conditions in the northernmost Nordic Seas. In this section, we will discuss the mechanisms associated with the identified modes of variability.

5.2.1 Mode I: strong oceanic heat release in the southeastern Nordic Seas

Mode I occurred toward the end of HS-4 (Fig. 4). During this period, the inflow of AW likely intensified due to a strong

335 AMOC. At the same time, little SIE remained in the southeastern Nordic Seas, with the sea ice margin reaching the Vøring Plateau (Sadatzki et al., 2019, 2020) (Fig. 4A). Sea ice is sensitive to both surface and subsurface ocean heat content (Polyakov et al., 2017; Docquier and Koenigk, 2021; Docquier et al., 2022). When the strong AW inflow reached the surface, it likely played a key role in preventing sea ice formation in the southeastern Nordic Seas.

Throughout the investigated period, 40–33.5 ka b2k, atmospheric temperatures were substantially lower than ocean

340 temperatures (≤-35°C) (Kindler et al., 2014). In ice-free areas south of the Vøring Plateau, oceanic heat transported by the AW was rapidly released to the atmosphere, as supported by the comparison of the southeast and northeast Nordic Seas SubST records (Figs. 4B & 5A). Before reaching the sea ice margin in the Vøring Plateau, the AW cooled enough to submerge, allowing sea ice to cover the northern Nordic Seas as far south as the Vøring Plateau (Fig. 6A).

5.2.2 Mode II: reduced heat transport and sea ice buildup across the eastern Nordic Seas

345 Mode II took place during late GI-7 and the subsequent GS-7 (Figs. 4 & 5B). A seasonal SIE was present from the southeastern Nordic Seas to the Fram Strait, regardless of whether it was during a GI or a GS.

During Mode II, an AMOC of intermediate strength likely reduced the oceanic heat transported via the AW inflow into the Nordic Seas, compared to the stronger AMOC state observed in Mode I. This reduction in ocean heat transport, indicated by the lowered SubSTs at MD99-2284 (Sadatzki et al., 2019) (Fig. 5A & B), was insufficient to trigger a year-round retreat of

350 sea ice in the southeastern Nordic Seas. As a result, the region remained seasonally ice-covered, with more sea ice accumulating farther north (Fig. 4A). Although seasonal cycles are expected, the AW submerged beneath the sea ice cover and halocline before reaching the Faeroe-Shetland Channel. This allowed heat to accumulate at intermediate depths across the Nordic Seas (e.g., Rasmussen and Thomsen, 2004; Dokken et al., 2013; Ezat et al., 2014; Sessford et al., 2019) (Fig. 6B). The relatively small difference in SubSTs between the southeastern (MD99-2284) and northern Nordic Seas (MD99-2304),

355 compared to Mode I, indicates that oceanic heat was more evenly distributed at intermediate depths within the Nordic Seas. Only slight heat loss occurred between the north and south (Figs. 4B & 5B). This supports the hypothesized existence of a homogeneous intermediate water mass occupying the Nordic Seas during GSs (Sessford et al., 2019).

Note that, while this interpretation aligns with indicated AMOC variability, the existing AMOC reconstruction (Henry et al., 2016) (Fig. 4C) lacks sufficient temporal resolution during GI-7 to provide direct support.

360 ### 5.2.3 Mode III: southern oceanic heat reservoir and northern polynyas

Mode III occurred during HS-4, late GI-8, and early GS-8 (Figs. 4 & 5C). This mode is associated with a weak AMOC (Fig. 4), which led to reduced ocean heat transport into the Nordic Seas. SubSTs, with values at intermediate levels in the

southeastern Nordic Seas (MD99-2284), were lower than those during Modes I and II (Sadatzki et al., 2019) (Fig. 4B). This reflects lower ocean heat contents in the region compared to the first two modes.

365 During these periods, extensive sea ice persisted in the southeastern Nordic Seas, where the AW submerged beneath the ice cover (Sadatzki et al., 2019, 2020) (Fig. 4A). Despite the overall reduction in northward ocean heat transport, heat still accumulated beneath the sea ice and halocline in this region. This heat content was then transported at intermediate depths along the NwAC pathway, forming a heat reservoir within the well-stratified eastern Nordic Seas (e.g., Rasmussen and Thomsen, 2004; Dokken et al., 2013; Ezat et al., 2014; Sessford et al., 2019).

370 In contrast to the southeastern Nordic Seas, nearly ice-free conditions are observed in the eastern Fram Strait. Wong et al. (2024) argued for polynya activity in the eastern Fram Strait during HS-4 under this same scenario. Furthermore, low SubSTs in the eastern Fram Strait (MD99-2304) (Figs. 4B & 5C) suggest ocean heat depletion.

Despite strong stratification in the eastern Nordic Seas, vertical mixing still occurred in its interior. One of the primary drivers of vertical mixing is the kinetic energy from variations in internal waves (Ferrari and Wunsch, 2009). Increased

375 vertical mixing can enhance the exchange of heat and salt between ocean layers (e.g., Liang and Losch, 2018; Beer et al., 2023; Saenz et al., 2023), hence, the warmer, saltier AW can be brought from intermediate depths to the surface, destabilizing the halocline on small spatial scales (e.g., Nguyen et al., 2009; Lind et al., 2016; Rheinländer et al., 2021). Since sea ice is sensitive to changes in surface and subsurface temperatures (Polyakov et al., 2017; Docquier and Koenigk, 2021; Docquier et al., 2022), upward heat fluxes can thus contribute to sea ice loss (e.g., Beer et al., 2023; Saenz et al.,

380 2023). Additionally, the much steeper continental slope in the eastern Fram Strait (Fig. 1), relative to the Vøring Plateau, may have played a key role in breaking internal waves (Falk-Petersen et al., 2015; Zhang et al., 2022). This process likely caused an upwelling of accumulated oceanic heat from the AW entering the eastern Fram Strait, thereby contributing to subsurface heat depletion and facilitating sea ice loss at MD99-2304 (Fig. 6C).

Hence, persistent sea ice cover and submerged AW inflow in the southeastern Nordic Seas likely contributed to the buildup

385 of an ocean heat reservoir at intermediate depths under a weak AMOC. We argue that vertical mixing in the eastern Fram Strait, possibly driven by interactions between internal waves and the steep continental slope, caused upwelling of stored heat. This process destabilized the halocline and eventually triggered the formation of seasonal polynyas at MD99-2304 (Wong et al., 2024).

5.2.4 Mode IV: strengthening ocean heat transport and increasing northern sea ice

390 Mode IV begins with a situation in which polynyas occurred in the eastern Fram Strait, while extensive sea ice covered the southeastern Nordic Seas. This mode is observed during GS-8 (Figs. 4 & 5D) when an intensifying AMOC gradually increased northward ocean heat transport. This strengthened heat transport, as evidenced by the increasing SubSTs at MD99-2284, entailed a gradual reduction in SIE in the southeastern Nordic Seas (Sadatzki et al., 2019, 2020) (Fig. 4 and 5D). As sea ice gradually disappeared from the region, the AW reached the surface (Dokken et al., 2013), releasing progressively

395 more oceanic heat to the colder atmosphere.

Sufficient ocean heat was lost in the southeastern Nordic Seas for the AW to be dense enough to submerge before reaching the eastern Fram Strait. Thereby, the coupled process of heat loss south of the Fram Strait and AW deepening contributed to gradual sea ice accumulation and decreasing SubSTs in the high north (Fig. 6D).

5.2.5 Mode V: strong northward ocean heat transport and sea ice retreat

400 Mode V features a nearly ice-free eastern Nordic Seas, from the south to the north, during early GI-8 and GI-7 (Figs. 4 & 5E).

The strong AMOC during these periods intensified the northward inflow of heat-laden AW. Oceanic heat reached the surface, with very little remaining in the subsurface, as indicated by low SubSTs in both the southeastern Nordic Seas (MD99-2284) (Sadatzki et al., 2019) and the eastern Fram Strait (MD99-2304) (Figs. 4B & 5E). This heat content

405 transferred freely to the atmosphere, accelerating atmospheric warming, with barely any sea ice to disrupt heat exchange. Once the atmospheric temperature reached a critical threshold, sea ice formation across the eastern Nordic Seas can be further inhibited, thus creating a positive feedback loop. These physical processes are supported by modern observations (e.g., Schlichtholz, 2011; Alexeev et al., 2017).

Mode V with a strong AMOC is associated with a seasonally ice-free eastern Nordic Seas, facilitating the release of oceanic

410 heat into the atmosphere. Among all modes investigated, this mode (Fig. 5E) most closely resembles modern-day surface and subsurface conditions in the eastern Nordic Seas, as discussed by e.g. Smedsrud et al. (2022). Both are characterized by a large ice-free surface, intense AW inflow, a weak halocline, and active upper ocean vertical mixing (Fig. 6E).
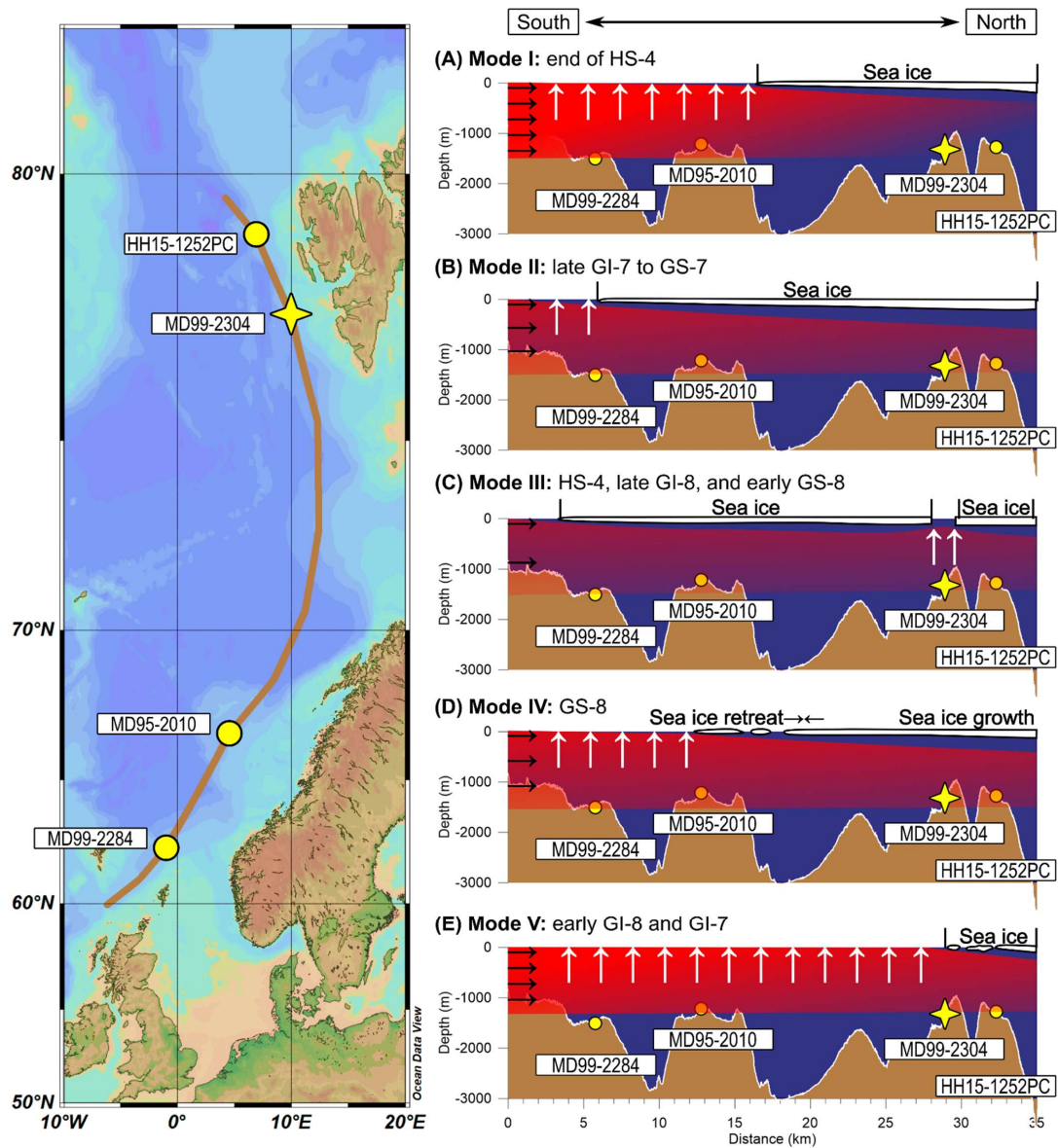
Figure 6. Schematic illustrating the relationship between the AMOC strength and SIE along the eastern Nordic Seas transect
under five modes: (A) Mode I – strong AMOC and perennial sea ice in the north, (B) Mode II – intermediate AMOC strength and

seasonal sea ice, (C) Mode III – weak AMOC and polynyas in the north, (D) Mode IV – strengthening AMOC and increasing sea ice in the north, and (E) Mode V – strong AMOC and seasonal sea ice in the north. The transect is indicated by the brown line in the left panel. The black rightward arrows indicate the AW and oceanic heat inflow, while the white upward arrows represent ocean heat release. The gradient from red to transparent shows oceanic heat loss in the AW. Bathymetry along the transect is

420   obtained from GEBCO (https://www.gebco.net/) and processed using QGIS (https://www.qgis.org/). The map is produced with Ocean Data View (https://odv.awi.de/), and the schematic is drawn using Inkscape software (http://www.inkscape.org/).

5.2.6 Other mechanisms

In addition to changes in ocean circulation, SIE in the Nordic Seas may have been influenced by prevailing atmospheric conditions, including atmospheric temperature changes and wind patterns. Records from Greenland indicate that atmospheric

425   temperatures display a comparable pattern of variability between and within individual GSs and GIs (Kindler et al., 2014; Rasmussen et al., 2014). SIE variability in the southeastern Nordic Seas (Sadatzki et al., 2019, 2020) and the North Atlantic (Scoto et al., 2022) aligns with the cycles observed in the D-O climate oscillations.

However, sea ice reconstructions from the southeastern Nordic Seas (Sadatzki et al., 2019, 2020), synchronized with Greenland records through the identification of microtephra layers (Berben et al., 2020), show that sea ice changes in the

430   Faroe-Shetland Channel preceded shifts in atmospheric temperatures over Greenland. This suggests that the atmospheric temperature changes were driven by sea ice variations, rather than the other way around.

Furthermore, since no reconstructions provide information on changing wind patterns or wind strengths for the investigated time interval, our study focuses on understanding the role of ocean circulation.

5.3 Implications of the eastern Fram Strait findings

435   The new data from MD99-2304 in the eastern Fram strait reveals clear intra-GS and intra-GI variability in SIE and SubSTs. Differences are also observed between the individual investigated GSs and GIs (Figs. 2 & 3). Most GSs and GIs during the investigated period experienced multiple modes of variability, with some modes confined within a single GS or GI. Others persisted from a GS into a GI or vice versa. These results document more variable GS and GI conditions in the northernmost Nordic Seas than previous conceptualizations, as earlier studies suggested that the northern Nordic Seas were permanently

440   covered by sea ice throughout GSs and GIs (e.g., Dokken et al., 2013; Sadatzki et al., 2019, 2020). Instead, our new findings suggest that the eastern Fram Strait polynyas during HS-4, identified by Wong et al. (2024), was not a unique example of more variable glacial conditions in the eastern Fram Strait. Beyond conditions comparable to the polynyas during HS-4 (Mode III), we document four other modes of variability that characterize GS and GI variability across the eastern Nordic Seas.

445   The GSs and GIs investigated in the eastern Fram Strait differed from the regularly repetitive pattern of the GS-GI oscillations in Greenland ice cores (Andersen et al., 2006; Rasmussen et al., 2014) (Figs. 2, 3, & S1). This indicates that the local variability in SIE and the associated release of oceanic heat observed in the eastern Fram Strait from our new

reconstructions had a minor impact on climate conditions over Greenland during GSs and GIs. In line with this interpretation, our records support previous studies arguing that sea ice conditions in the southeastern Nordic Seas and the North Atlantic were driving atmospheric changes over Greenland through ocean-ice-atmosphere interactions (Jansen et al., 2020; Sadatzki et al., 2020; Buizert et al., 2024).

6 Conclusions

Our proxy results from MD99-2304 reveal clear variability in SIE and SubSTs in the eastern Fram Strait between and within individual GSs and GIs between 40 and 33.5 ka b2k. The intra-GS and -GI variability was not reflected in the climate records from the Greenland ice cores. Compared to SIE and SubSTs conditions in the eastern Fram Strait, changes in the southeastern Nordic Seas and the North Atlantic were more closely linked to climate variations over Greenland.

Fluctuations in SIE and SubSTs in the eastern Fram Strait were primarily driven by northward oceanic heat transport, which was strongly influenced by the strength of the AMOC and sea ice conditions in the southeastern Nordic Seas. Based on these findings, we identify five distinct modes describing the interplay between SIE, SubSTs, and AMOC strength across the eastern Nordic Seas.

Acknowledgements

We thank the crew of cruise Marion Dufresne IMAGES 5 1999 for retrieving Core MD99-2304 on leg MD114. We also thank Dag Inge Blindheim of NORCE for assisting with the foraminifera analysis, Walter Luttmer of AWI for assisting with the biomarker and TOC measurements, Defang You and Wee Wei Khoo of AWI for assisting with the biomarker measurements, Valéa Schumacher, Frederike Schmidt, Anja Müller, Amelie Nübel, Jens Strauss, and Justin Lindemann of AWI for assisting with the TOC measurements and analytical discussion of TOC measurement techniques. This research is funded by the Research Council of Norway (RCN) through project ABRUPT Arctic Climate Change (project number 325333).

Data availability

The MD99-2304 biomarker and $Mg/Ca_{N.p}$ datasets are uploaded to pangaea.de and will be made available upon publication.

Author contribution

Wanyee Wong: Conceptualization, Methodology, Validation, Formal analysis, Investigation, Data Curation, Writing – original draft, Writing – review & editing, Visualization. Bjørg Risebrobakken: Conceptualization, Investigation, Resources, Writing – original draft, Writing – review & editing, Visualization, Supervision, Project administration, Funding acquisition.

475 Malin Ödalen: Conceptualization, Investigation, Writing – original draft, Writing – review & editing, Visualization. Amandine Aline Tisserand: Methodology, Validation, Formal analysis, Data Curation, Writing – review & editing. Kirsten Fahl: Methodology, Validation, Formal analysis, Resources, Data Curation, Writing – review & editing, Supervision. Ruediger Stein: Methodology, Formal analysis, Investigation, Writing – review & editing, Visualization, Supervision. Eystein Jansen: Investigation, Writing – review & editing, Supervision.

480 **References**

Alexeev, V.A., Walsh, J.E., Ivanov, V. V, Semenov, V.A., Smirnov, A. V, 2017. Warming in the Nordic Seas, North Atlantic storms and thinning Arctic sea ice. Environmental Research Letters 12, 084011. https://doi.org/10.1088/1748-9326/aa7a1d

Andersen, K.K., Svensson, A., Johnsen, S.J., Rasmussen, S.O., Bigler, M., Röthlisberger, R., Ruth, U., Siggaard-Andersen,

485 M.L., Peder Steffensen, J., Dahl-Jensen, D., Vinther, B.M., Clausen, H.B., 2006. The Greenland Ice Core Chronology 2005, 15-42 ka. Part 1: constructing the time scale. Quat Sci Rev 25, 3246–3257. https://doi.org/10.1016/j.quascirev.2006.08.002

Årthun, M., Eldevik, T., 2016. On Anomalous Ocean Heat Transport toward the Arctic and Associated Climate Predictability. J Clim 29, 689–704. https://doi.org/10.1175/JCLI-D-15-0448.1

490 Årthun, M., Eldevik, T., Smedsrud, L.H., 2019. The Role of Atlantic Heat Transport in Future Arctic Winter Sea Ice Loss. J Clim 32, 3327–3341. https://doi.org/10.1175/JCLI-D-18-0750.1

Barker, S., Greaves, M., Elderfield, H., 2003. A study of cleaning procedures used for foraminiferal Mg/Ca paleothermometry. Geochemistry, Geophysics, Geosystems 4. https://doi.org/10.1029/2003GC000559

Beer, E., Eisenman, I., Wagner, T.J.W., Fine, E.C., 2023. A Possible Hysteresis in the Arctic Ocean due to Release of

495 Subsurface Heat during Sea Ice Retreat. J Phys Oceanogr 53, 1323–1335. https://doi.org/10.1175/JPO-D-22-0131.1

Belt, S.T., Allard, W.G., Massé, G., Robert, J.-M., Rowland, S.J., 2000. Highly branched isoprenoids (HBIs): identification of the most common and abundant sedimentary isomers. Geochim Cosmochim Acta 64, 3839–3851. https://doi.org/10.1016/S0016-7037(00)00464-6

Belt, S.T., Massé, G., Rowland, S.J., Poulin, M., Michel, C., LeBlanc, B., 2007. A novel chemical fossil of palaeo sea ice:

500 IP25. Org Geochem 38, 16–27. https://doi.org/10.1016/j.orggeochem.2006.09.013

Bensi, M., Kovačević, V., Langone, L., Aliani, S., Ursella, L., Goszczko, I., Soltwedel, T., Skogseth, R., Nilsen, F., Deponte, D., Mansutti, P., Laterza, R., Rebesco, M., Rui, L., Lucchi, R.G., Wåhlin, A., Viola, A., Beszczynska-Möller, A., Rubino, A., 2019. Deep Flow Variability Offshore South-West Svalbard (Fram Strait). Water (Basel) 11, 683. https://doi.org/10.3390/w11040683

505 Berben, S.M.P., Dokken, T.M., Abbott, P.M., Cook, E., Sadatzki, H., Simon, M.H., Jansen, E., 2020. Independent tephrochronological evidence for rapid and synchronous oceanic and atmospheric temperature rises over the Greenland

stadial-interstadial transitions between ca. 32 and 40 ka b2k. Quat Sci Rev 236. https://doi.org/10.1016/j.quascirev.2020.106277

Blindheim, J., Østerhus, S., 2005. The Nordic seas, main oceanographic features. pp. 11–37. https://doi.org/10.1029/158GM03

Boon, J.J., Rijpstra, W.I.C., de Lange, F., de Leeuw, J.W., Yoshioka, M., Shimizu, Y., 1979. Black Sea sterol—a molecular fossil for dinoflagellate blooms. Nature 277, 125–127. https://doi.org/10.1038/277125a0

Bosse, A., Fer, I., Søiland, H., Rossby, T., 2018. Atlantic Water Transformation Along Its Poleward Pathway Across the Nordic Seas. J Geophys Res Oceans 123, 6428–6448. https://doi.org/10.1029/2018JC014147

Boyle, E.A., 1981. Cadmium, zinc, copper, and barium in foraminifera tests. Earth Planet Sci Lett 53, 11–35. https://doi.org/10.1016/0012-821X(81)90022-4

Boyle, E.A., Keigwin, L.D., 1985. Comparison of Atlantic and Pacific paleochemical records for the last 215,000 years: changes in deep ocean circulation and chemical inventories. Earth Planet Sci Lett 76, 135–150. https://doi.org/10.1016/0012-821X(85)90154-2

Bradtmiller, L.I., McManus, J.F., Robinson, L.F., 2014. 231Pa/230Th evidence for a weakened but persistent Atlantic meridional overturning circulation during Heinrich Stadial 1. Nat Commun 5, 5817. https://doi.org/10.1038/ncomms6817

Bryden, H.L., 2021. Wind-driven and buoyancy-driven circulation in the subtropical North Atlantic Ocean. Proceedings of the Royal Society A: Mathematical, Physical and Engineering Sciences 477. https://doi.org/10.1098/rspa.2021.0172

Buizert, C., Sowers, T.A., Niezgoda, K., Blunier, T., Gkinis, V., Harlan, M., He, C., Jones, T.R., Kjaer, H.A., Liisberg, J.B., Menking, J.A., Morris, V., Noone, D., Rasmussen, S.O., Sime, L.C., Steffensen, J.P., Svensson, A., Vaughn, B.H., Vinther, B.M., White, J.W.C., 2024. The Greenland spatial fingerprint of Dansgaard–Oeschger events in observations and models. Proceedings of the National Academy of Sciences 121. https://doi.org/10.1073/pnas.2402637121

Cuny, J., Rhines, P.B., Niiler, P.P., Bacon, S., 2002. Labrador Sea Boundary Currents and the Fate of the Irminger Sea Water. J Phys Oceanogr 32, 627–647. https://doi.org/10.1175/1520-0485(2002)032<0627:LSBCAT>2.0.CO;2

Dansgaard, W., Clausen, H.B., Gundestrup, N., Hammer, C.U., Johnsen, S.F., Kristinsdottir, P.M., Reeh, N., 1982. A New Greenland Deep Ice Core. Science (1979) 218. https://doi.org/10.1126/science.218.4579.1273

Day, J.J., Hargreaves, J.C., Annan, J.D., Abe-Ouchi, A., 2012. Sources of multi-decadal variability in Arctic sea ice extent. Environmental Research Letters 7, 034011. https://doi.org/10.1088/1748-9326/7/3/034011

Docquier, D., Koenigk, T., 2021. A review of interactions between ocean heat transport and Arctic sea ice. Environmental Research Letters 16, 123002. https://doi.org/10.1088/1748-9326/ac30be

Docquier, D., Vannitsem, S., Ragone, F., Wyser, K., Liang, X.S., 2022. Causal Links Between Arctic Sea Ice and Its Potential Drivers Based on the Rate of Information Transfer. Geophys Res Lett 49. https://doi.org/10.1029/2021GL095892

540 Dokken, T.M., Nisancioglu, K.H., Li, C., Battisti, D.S., Kissel, C., 2013. Dansgaard-Oeschger cycles: Interactions between ocean and sea ice intrinsic to the Nordic seas. Paleoceanography 28, 491–502. https://doi.org/10.1002/palo.20042

El bani Altuna, N., Ezat, M.M., Smik, L., Muschitiello, F., Belt, S.T., Knies, J., Rasmussen, T.L., 2024. Sea ice-ocean coupling during Heinrich Stadials in the Atlantic–Arctic gateway. Sci Rep 14, 1065. https://doi.org/10.1038/s41598-024-51532-7

545 Elderfield, H., Ganssen, G., 2000. Past temperature and δ18O of surface ocean waters inferred from foraminiferal Mg/Ca ratios. Nature 405, 442–445. https://doi.org/10.1038/35013033

Ezat, M.M., Rasmussen, T.L., Groeneveld, J., 2016. Reconstruction of hydrographic changes in the southern Norwegian Sea during the past 135 kyr and the impact of different foraminiferal Mg/Ca cleaning protocols. Geochemistry, Geophysics, Geosystems 17, 3420–3436. https://doi.org/10.1002/2016GC006325

550 Ezat, M.M., Rasmussen, T.L., Groeneveld, J., 2014. Persistent intermediate water warming during cold stadials in the southeastern Nordic seas during the past 65 k.y. Geology 42, 663–666. https://doi.org/10.1130/G35579.1

Fahl, K., Stein, R., 2012. Modern seasonal variability and deglacial/Holocene change of central Arctic Ocean sea-ice cover: New insights from biomarker proxy records. Earth Planet Sci Lett 351–352, 123–133. https://doi.org/10.1016/j.epsl.2012.07.009

555 Fahrbach, Eberhard, Meincke, J., Østerhus, S., Rohardt, Gerd, Schauer, Ursula, Tverberg, V., Verduin, Jennifer, Fahrbach, E, Rohardt, G, Schauer, U, Verduin, J, 2001. Direct measurements of volume transports through Fram Strait, Polar Research.

Falk-Petersen, S., Pavlov, V., Berge, J., Cottier, F., Kovacs, K.M., Lydersen, C., 2015. At the rainbow's end: high productivity fueled by winter upwelling along an Arctic shelf. Polar Biol 38, 5–11. https://doi.org/10.1007/s00300-560 014-1482-1

Ferrari, R., Wunsch, C., 2009. Ocean Circulation Kinetic Energy: Reservoirs, Sources, and Sinks. Annu Rev Fluid Mech 41, 253–282. https://doi.org/10.1146/annurev.fluid.40.111406.102139

Florence, F., Walt, M., Matt, S., Ann, W., 2017. Sea Ice Index, Version 3. National Snow and Ice Data Center.

Furevik, T., 2001. Annual and interannual variability of Atlantic Water temperatures in the Norwegian and Barents Seas: 565 1980}1996, Deep-Sea Research I.

Gordon, A.L., 1986. Interocean exchange of thermocline water. J Geophys Res Oceans 91, 5037–5046. https://doi.org/10.1029/JC091iC04p05037

Govin, A., Braconnot, P., Capron, E., Cortijo, E., Duplessy, J.-C., Jansen, E., Labeyrie, L., Landais, A., Marti, O., Michel, E., Mosquet, E., Risebrobakken, B., Swingedouw, D., Waelbroeck, C., 2012. Persistent influence of ice sheet melting 570 on high northern latitude climate during the early Last Interglacial. Climate of the Past 8, 483–507. https://doi.org/10.5194/cp-8-483-2012

Hall, M.M., Bryden, H.L., 1982. Direct estimates and mechanisms of ocean heat transport. Deep Sea Research Part A. Oceanographic Research Papers 29, 339–359. https://doi.org/10.1016/0198-0149(82)90099-1

Hattermann, T., Isachsen, P.E., von Appen, W.J., Albretsen, J., Sundfjord, A., 2016. Eddy-driven recirculation of Atlantic
575   Water in Fram Strait. Geophys Res Lett 43, 3406–3414. https://doi.org/10.1002/2016GL068323

Henry, L.G., McManus, J.F., Curry, W.B., Roberts, N.L., Piotrowski, A.M., Keigwin, L.D., 2016. North Atlantic ocean
           circulation   and   abrupt   climate   change   during   the   last   glaciation.   Science   (1979)   353.
           https://doi.org/10.1126/science.aaf5529

Hoff, U., Rasmussen, T.L., Stein, R., Ezat, M.M., Fahl, K., 2016. Sea ice and millennial-scale climate variability in the
580   Nordic seas 90 kyr ago to present. Nat Commun 7. https://doi.org/10.1038/ncomms12247

Holliday, N.P., Meyer, A., Bacon, S., Alderson, S.G., de Cuevas, B., 2007. Retroflection of part of the east Greenland
           current at Cape Farewell. Geophys Res Lett 34. https://doi.org/10.1029/2006GL029085

Ingvaldsen, R.B., 2005. Width of the North Cape Current and location of the Polar Front in the western Barents Sea.
           Geophys Res Lett 32. https://doi.org/10.1029/2005GL023440

585 Jansen, E., Christensen, J.H., Dokken, T., Nisancioglu, K.H., Vinther, B.M., Capron, E., Guo, C., Jensen, M.F., Langen,
           P.L., Pedersen, R.A., Yang, S., Bentsen, M., Kjær, H.A., Sadatzki, H., Sessford, E., Stendel, M., 2020. Past
           perspectives   on   the   present   era   of   abrupt   Arctic   climate   change.   Nat   Clim   Chang   10,   714–721.
           https://doi.org/10.1038/s41558-020-0860-7

Jones, C.S., Jiang, S., Abernathey, R.P., 2024. A Comparison of Diagnostics for AMOC Heat Transport Applied to the
590   CESM Large Ensemble. J Adv Model Earth Syst 16. https://doi.org/10.1029/2023MS003978

Kindler, P., Guillevic, M., Baumgartner, M., Schwander, J., Landais, A., Leuenberger, M., 2014. Temperature reconstruction
           from 10 to 120 kyr b2k from the NGRIP ice core. Climate of the Past 10, 887–902. https://doi.org/10.5194/cp-10-887-
           2014

Kissel, C., Laj, C., Labeyrie, L., Dokken, T., Voelker, A., Blamart, D., 1999. Rapid climatic variations during marine
595   isotopic stage 3: Magnetic analysis of sediments from Nordic Seas and North Atlantic. Earth Planet Sci Lett 171, 489–
           502. https://doi.org/10.1016/S0012-821X(99)00162-4

Kolling, H.M., Stein, R., Fahl, K., Sadatzki, H., de Vernal, A., Xiao, X., 2020. Biomarker Distributions in (Sub)-Arctic
           Surface Sediments and Their Potential for Sea Ice Reconstructions. Geochemistry, Geophysics, Geosystems 21.
           https://doi.org/10.1029/2019GC008629

600 Köseoğlu, D., Belt, S.T., Husum, K., Knies, J., 2018. An assessment of biomarker-based multivariate classification methods
           versus   the   PIP25   index   for   paleo   Arctic   sea   ice   reconstruction.   Org   Geochem   125,   82–94.
           https://doi.org/10.1016/j.orggeochem.2018.08.014

Larson, S.M., Buckley, M.W., Clement, A.C., 2020. Extracting the Buoyancy-Driven Atlantic Meridional Overturning
           Circulation. J Clim 33, 4697–4714. https://doi.org/10.1175/JCLI-D-19-0590.1

605 Li, C., Born, A., 2019. Coupled atmosphere-ice-ocean dynamics in Dansgaard-Oeschger events. Quat Sci Rev.
           https://doi.org/10.1016/j.quascirev.2018.10.031

Liang, X., Losch, M., 2018. On the Effects of Increased Vertical Mixing on the Arctic Ocean and Sea Ice. J Geophys Res Oceans 123, 9266–9282. https://doi.org/10.1029/2018JC014303

Lind, S., Ingvaldsen, R.B., Furevik, T., 2016. Arctic layer salinity controls heat loss from deep Atlantic layer in seasonally ice-covered areas of the Barents Sea. Geophys Res Lett 43, 5233–5242. https://doi.org/10.1002/2016GL068421

Liu, W., Xie, S.-P., Liu, Z., Zhu, J., 2017. Overlooked possibility of a collapsed Atlantic Meridional Overturning Circulation in warming climate. Sci Adv 3. https://doi.org/10.1126/sciadv.1601666

Lozier, M.S., Li, F., Bacon, S., Bahr, F., Bower, A.S., Cunningham, S.A., de Jong, M.F., de Steur, L., deYoung, B., Fischer, J., Gary, S.F., Greenan, B.J.W., Holliday, N.P., Houk, A., Houpert, L., Inall, M.E., Johns, W.E., Johnson, H.L., Johnson, C., Karstensen, J., Koman, G., Le Bras, I.A., Lin, X., Mackay, N., Marshall, D.P., Mercier, H., Oltmanns, M., Pickart, R.S., Ramsey, A.L., Rayner, D., Straneo, F., Thierry, V., Torres, D.J., Williams, R.G., Wilson, C., Yang, J., Yashayaev, I., Zhao, J., 2019. A sea change in our view of overturning in the subpolar North Atlantic. Science (1979) 363, 516–521. https://doi.org/10.1126/science.aau6592

Mahajan, S., Zhang, R., Delworth, T.L., 2011. Impact of the Atlantic Meridional Overturning Circulation (AMOC) on Arctic Surface Air Temperature and Sea Ice Variability. J Clim 24, 6573–6581. https://doi.org/10.1175/2011JCLI4002.1

Mandal, G., Hettiarachchi, A.I., Ekka, S. V., 2024. The North Atlantic subpolar ocean dynamics during the past 21,000 years. Dynamics of Atmospheres and Oceans 106, 101462. https://doi.org/10.1016/j.dynatmoce.2024.101462

Martin, P.A., Lea, D.W., 2002. A simple evaluation of cleaning procedures on fossil benthic foraminiferal Mg/Ca. Geochemistry, Geophysics, Geosystems 3, 1–8. https://doi.org/10.1029/2001GC000280

Missiaen, L., Bouttes, N., Roche, D.M., Dutay, J.-C., Quiquet, A., Waelbroeck, C., Pichat, S., Peterschmitt, J.-Y., 2020. Carbon isotopes and Pa∕Th response to forced circulation changes: a model perspective. Climate of the Past 16, 867–883. https://doi.org/10.5194/cp-16-867-2020

Mogensen, I.A., 2009. Dansgaard-Oeschger Cycles, in: Encyclopedia of Paleoclimatology and Ancient Environments. Springer Netherlands, Dordrecht, pp. 229–233. https://doi.org/10.1007/978-1-4020-4411-3_55

Morley, A., de la Vega, E., Raitzsch, M., Bijma, J., Ninnemann, U., Foster, G.L., Chalk, T.B., Meilland, J., Cave, R.R., Büscher, J. V., Kucera, M., 2024. A solution for constraining past marine Polar Amplification. Nat Commun 15, 9002. https://doi.org/10.1038/s41467-024-53424-w

Müller, J., Wagner, A., Fahl, K., Stein, R., Prange, M., Lohmann, G., 2011. Towards quantitative sea ice reconstructions in the northern North Atlantic: A combined biomarker and numerical modelling approach. Earth Planet Sci Lett 306, 137–148. https://doi.org/10.1016/j.epsl.2011.04.011

Nguyen, A.T., Menemenlis, D., Kwok, R., 2009. Improved modeling of the Arctic halocline with a subgrid-scale brine rejection parameterization. J Geophys Res Oceans 114. https://doi.org/10.1029/2008JC005121

North Greenland Ice Core Project members, 2004. High-resolution record of Northern Hemisphere climate extending into the last interglacial period. Nature 431, 147–151. https://doi.org/10.1038/nature02805

640 Orvik, K.A., Niiler, P., 2002. Major pathways of Atlantic water in the northern North Atlantic and Nordic Seas toward Arctic. Geophys Res Lett 29. https://doi.org/10.1029/2002GL015002

Pedro, J.B., Andersson, C., Vettoretti, G., Voelker, A.H.L., Waelbroeck, C., Dokken, T.M., Jensen, M.F., Rasmussen, S.O., Sessford, E.G., Jochum, M., Nisancioglu, K.H., 2022. Dansgaard-Oeschger and Heinrich event temperature anomalies in the North Atlantic set by sea ice, frontal position and thermocline structure. Quat Sci Rev 289.
645 https://doi.org/10.1016/j.quascirev.2022.107599

Petit, T., Lozier, M.S., Josey, S.A., Cunningham, S.A., 2021. Role of air–sea fluxes and ocean surface density in the production of deep waters in the eastern subpolar gyre of the North Atlantic. Ocean Science 17, 1353–1365. https://doi.org/10.5194/os-17-1353-2021

Polyakov, I. V., Pnyushkov, A. V., Alkire, M.B., Ashik, I.M., Baumann, T.M., Carmack, E.C., Goszczko, I., Guthrie, J.,
650 Ivanov, V. V., Kanzow, T., Krishfield, R., Kwok, R., Sundfjord, A., Morison, J., Rember, R., Yulin, A., 2017. Greater role for Atlantic inflows on sea-ice loss in the Eurasian Basin of the Arctic Ocean. Science (1979) 356, 285–291. https://doi.org/10.1126/science.aai8204

Poulain, P.M., Warn-Varnas, A., Niiler, P.P., 1996. Near-surface circulation of the Nordic seas as measured by Lagrangian drifters. J Geophys Res Oceans 101, 18237–18258. https://doi.org/10.1029/96JC00506

655 Rasmussen, S.O., Bigler, M., Blockley, S.P., Blunier, T., Buchardt, S.L., Clausen, H.B., Cvijanovic, I., Dahl-Jensen, D., Johnsen, S.J., Fischer, H., Gkinis, V., Guillevic, M., Hoek, W.Z., Lowe, J.J., Pedro, J.B., Popp, T., Seierstad, I.K., Steffensen, J.P., Svensson, A.M., Vallelonga, P., Vinther, B.M., Walker, M.J.C., Wheatley, J.J., Winstrup, M., 2014. A stratigraphic framework for abrupt climatic changes during the Last Glacial period based on three synchronized Greenland ice-core records: Refining and extending the INTIMATE event stratigraphy. Quat Sci Rev 106, 14–28.
660 https://doi.org/10.1016/j.quascirev.2014.09.007

Rasmussen, T.L., Thomsen, E., 2004. The role of the North Atlantic Drift in the millennial timescale glacial climate fluctuations. Palaeogeogr Palaeoclimatol Palaeoecol 210, 101–116. https://doi.org/10.1016/j.palaeo.2004.04.005

Rhein, M., Kieke, D., Hüttl-Kabus, S., Roessler, A., Mertens, C., Meissner, R., Klein, B., Böning, C.W., Yashayaev, I., 2011. Deep water formation, the subpolar gyre, and the meridional overturning circulation in the subpolar North
665 Atlantic. Deep Sea Research Part II: Topical Studies in Oceanography 58, 1819–1832. https://doi.org/10.1016/j.dsr2.2010.10.061

Rheinlænder, J.W., Smedsrud, L.H., Nisanciouglu, K.H., 2021. Internal Ocean Dynamics Control the Long-Term Evolution of Weddell Sea Polynya Activity. Frontiers in Climate 3. https://doi.org/10.3389/fclim.2021.718016

Robinson, L.F., Henderson, G.M., Ng, H.C., McManus, J.F., 2019. Pa/Th as a (paleo)circulation tracer: A North Atlantic
670 perspective. Past Global Changes Magazine 27. https://doi.org/10.22498/pages.27.2.56

Sadatzki, H., Dokken, T.M., Berben, S.M.P., Muschitiello, F., Stein, R., Fahl, K., Menviel, L., Timmermann, A., Jansen, E., 2019. Sea ice variability in the southern Norwegian Sea during glacial Dansgaard-Oeschger climate cycles. Sci Adv 5. https://doi.org/10.1126/sciadv.aau6174

Sadatzki, H., Maffezzoli, N., Dokken, T.M., Simon, M.H., Berben, S.M.P., Fahl, K., Kjær, H.A., Spolaor, A., Stein, R.,
675   Vallelonga, P., Vinther, B.M., Jansen, E., 2020. Rapid reductions and millennial-scale variability in Nordic Seas sea
ice cover during abrupt glacial climate changes. Proceedings of the National Academy of Sciences 117, 29478–29486.
https://doi.org/10.1073/pnas.2005849117

Saenz, B.T., McKee, D.C., Doney, S.C., Martinson, D.G., Stammerjohn, S.E., 2023. Influence of seasonally varying sea-ice
concentration and subsurface ocean heat on sea-ice thickness and sea-ice seasonality for a 'warm-shelf' region in
680   Antarctica. Journal of Glaciology 69, 1466–1482. https://doi.org/10.1017/jog.2023.36

Schlichtholz, P., 2011. Influence of oceanic heat variability on sea ice anomalies in the Nordic Seas. Geophys Res Lett 38.
https://doi.org/10.1029/2010GL045894

Scoto, F., Sadatzki, H., Maffezzoli, N., Barbante, C., Gagliardi, A., Varin, C., Vallelonga, P., Gkinis, V., Dahl-Jensen, D.,
Kjær, H.A., Burgay, F., Saiz-Lopez, A., Stein, R., Spolaor, A., 2022. Sea ice fluctuations in the Baffin Bay and the
685   Labrador Sea during glacial abrupt climate changes. Proceedings of the National Academy of Sciences 119.
https://doi.org/10.1073/pnas.2203468119

Sessford, E.G., Jensen, M.F., Tisserand, A.A., Muschitiello, F., Dokken, T., Nisancioglu, K.H., Jansen, E., 2019. Consistent
fluctuations in intermediate water temperature off the coast of Greenland and Norway during Dansgaard-Oeschger
events. Quat Sci Rev 223. https://doi.org/10.1016/j.quascirev.2019.105887

690 Smedsrud, L.H., Muilwijk, M., Brakstad, A., Madonna, E., Lauvset, S.K., Spensberger, C., Born, A., Eldevik, T., Drange,
H., Jeansson, E., Li, C., Olsen, A., Skagseth, Ø., Slater, D.A., Straneo, F., Våge, K., Årthun, M., 2022. Nordic Seas
Heat Loss, Atlantic Inflow, and Arctic Sea Ice Cover Over the Last Century. Reviews of Geophysics.
https://doi.org/10.1029/2020RG000725

Stein, R., Fahl, K., Gierz, P., Niessen, F., Lohmann, G., 2017. Arctic Ocean sea ice cover during the penultimate glacial and
695   the last interglacial. Nat Commun 8. https://doi.org/10.1038/s41467-017-00552-1

Sun, J., Latif, M., Park, W., 2021. Subpolar Gyre – AMOC – Atmosphere Interactions on Multidecadal Timescales in a
Version of the Kiel Climate Model. J Clim 1–56. https://doi.org/10.1175/JCLI-D-20-0725.1

van der Linden, E.C., Le Bars, D., Bintanja, R., Hazeleger, W., 2019. Oceanic heat transport into the Arctic under high and
low CO 2 forcing. Clim Dyn 53, 4763–4780. https://doi.org/10.1007/s00382-019-04824-y

700 Volkman, J.K., 1986. A review of sterol markers for marine and terrigenous organic matter. Org Geochem 9, 83–99.
https://doi.org/10.1016/0146-6380(86)90089-6

Wong, W., Risebrobakken, B., Fahl, K., Stein, R., Jansen, E., Steinsland, K., Kissel, C., 2024. Sea ice in the Nordic Seas:
Greenland stadial to interstadial changes. Quat Sci Rev 343, 108916. https://doi.org/10.1016/j.quascirev.2024.108916

Xiao, X., Fahl, K., Müller, J., Stein, R., 2015. Sea-ice distribution in the modern Arctic Ocean: Biomarker records from
705   trans-Arctic Ocean surface sediments. Geochim Cosmochim Acta 155, 16–29.
https://doi.org/10.1016/J.GCA.2015.01.029

Yu, J., Anderson, R.F., Jin, Z.D., Ji, X., Thornalley, D.J.R., Wu, L., Thouveny, N., Cai, Y., Tan, L., Zhang, F., Menviel, L., Tian, J., Xie, X., Rohling, E.J., McManus, J.F., 2023. Millennial atmospheric CO2 changes linked to ocean ventilation modes over past 150,000 years. Nat Geosci 16, 1166–1173. https://doi.org/10.1038/s41561-023-01297-x

710   Zhang, S., Wu, L., Arnqvist, J., Hallgren, C., Rutgersson, A., 2022. Mapping coastal upwelling in the Baltic Sea from 2002 to 2020 using remote sensing data. International Journal of Applied Earth Observation and Geoinformation 114, 103061. https://doi.org/10.1016/j.jag.2022.103061